Solar Energy Materials & Solar Cells 95 (2011) 2632–2637

Contents lists available at ScienceDirect

Solar Energy Materials & Solar Cells

journal homepage: www.elsevier.com/locate/solmat

Distinguishing morphological and electrical defects in polycrystalline silicon solar cells using scanning electron acoustic microscopy and electron beam induced current

L. Meng [a,*], D. Nagalingam [a], C.S. Bhatia [a], A.G. Street [b,c], J.C.H. Phang [a,c]

[a] Centre for Integrated Circuit Failure Analysis and Reliability (CICFAR), Department of Electrical and Computer Engineering, National University of Singapore, 4 Engineering Drive 3, Singapore 117576, Singapore
[b] Qualcomm CDMA Technologies, 5775 Morehouse Drive, San Diego, CA 92121, USA
[c] Inscope Labs Pte Ltd., 28 Ayer Rajah Crescent # 03-01, Singapore 139959, Singapore

ARTICLE INFO

Article history:
Received 21 December 2010
Accepted 12 May 2011

Keywords:
Morphological defect
Electrical defect
Solar cell
Scanning Electron Acoustic Microscopy
Electron Beam Induced Current

ABSTRACT

Morphological and electrical defects in polycrystalline silicon solar cells are distinguished by scanning electron acoustic microscopy (SEAM) and electron beam induced current (EBIC) techniques, respectively. It was found that while some defects are both morphologically and electrically detectable, some are predominantly only either electrical or morphological in nature. Combining both SEAM and EBIC is therefore an ideal approach as the two techniques can provide complementary information on both the morphological and electrical manifestation of the defects.

1. Introduction

Polycrystalline silicon (poly-Si) is a promising candidate for low cost and large area solar cells. However, one major limitation of poly-Si solar cells, as compared to their counterparts made of single crystal Si, is their low efficiencies. The poor performance of these cells is attributed to the existence of morphological and electrical defects [1]. For the investigation of morphological defects, scanning electron acoustic microscopy (SEAM) is a preferred tool due to its non-destructive nature, its ability of subsurface imaging and depth profiling, as well as the ease in sample preparation [2,3]. SEAM, however, is not sensitive to non-morphological electrical defects, i.e. electrical defects without morphological features. In addition, even within a single morphological defect, the electrical properties may vary at different locations [4]. On the other hand, electron beam induced current (EBIC) is an ideal technique for characterization of electrical defects such as recombination sites, doping level inhomogeneities [5] and electrical irregularities in solar cells [6]. However, EBIC requires a pn junction and the detection range is limited to a few diffusion lengths from the junction. In other words, electrical defects that are further away from the junction cannot be revealed by the EBIC technique.

In this paper, we have utilized both SEAM and EBIC as complementary methods for characterization of defects in poly-Si solar cells. Morphological and electrical defects in a poly-Si solar cell were first distinguished by SEAM and EBIC, respectively. We would subsequently show that a defect could be predominantly morphological in nature (as revealed by SEAM) and yet electrically undetectable (by EBIC), and vice versa. This implies that neither SEAM nor EBIC alone is enough for the defect investigation; combining both SEAM and EBIC is a better approach instead as the two techniques can provide complementary information on both the electrical and morphological manifestation of the defects.

2. Experimental setup

A Hitachi S2700 scanning electron microscope (SEM) is modified for both SEAM and EBIC imaging. Fig. 1 shows the block diagram of the SEAM and EBIC setups. For the SEAM setup, an intensity-modulated electron beam is achieved with the beam blanking system that comprises a function generator, amplifier and blanking plates [7]. When the modulated electron beam irradiates the sample surface, localized heating induces acoustic waves that propagate through the sample and are detected by

* Corresponding author. Tel.: +65 6516 1568; fax: +65 6516 7912.
E-mail address: lei.meng@nus.edu.sg (L. Meng).

0927-0248/$ - see front matter © 2011 Elsevier B.V. All rights reserved.
doi:10.1016/j.solmat.2011.05.022

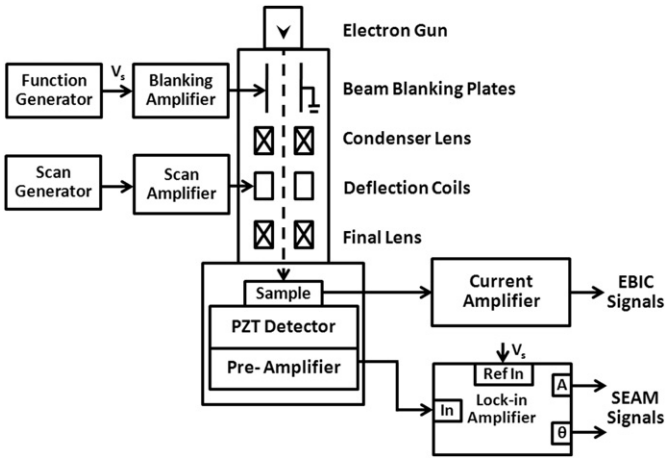

Fig. 1. SEAM and EBIC experimental setup.

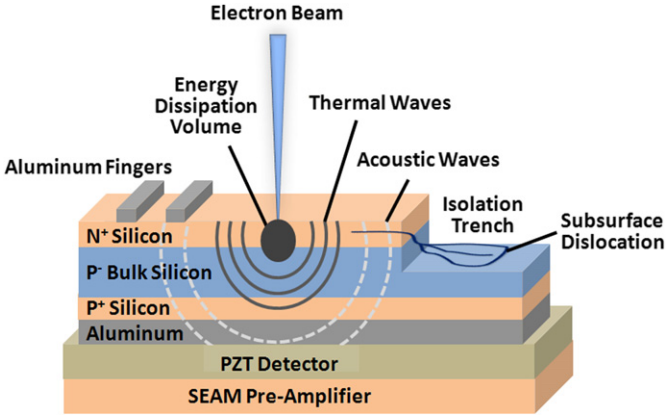

Fig. 2. SEAM signal detection of the solar cell.

a lead zirconate titanate (PZT) piezoelectric transducer attached to the backside of the sample. The PZT transducer converts the acoustic waves into electrical signals, which are amplified and fed into a lock-in amplifier (LIA). The reference of the LIA is the same signal that is used to drive the blanking plates of the SEM. The LIA outputs comprise both SEAM amplitude (A) and phase (θ) signals. An active imaging system, SEMICAPS 2200A, is used to generate SEAM amplitude (A) and phase (θ) images by synchronizing the scan generator with the output of the LIA. EBIC imaging is performed with the beam blanking system turned off. The EBIC current is amplified with a low noise current amplifier. The same active imaging system is used to generate EBIC images from the output of the current amplifier.

Figs. 2 and 3 show the SEAM and EBIC signal detection, respectively, each illustrated with the aid of an isometric view of the poly-Si solar cells used in this project. The poly-Si solar cells were fabricated by growing a 0.6 μm thick n^+ Si epitaxial layer on a 200 μm thick p^- silicon substrate. Each solar cell sample consists of several photovoltaic cells that are separated from one another by 2 μm deep isolation trenches. For SEAM imaging, as the modulated electron beam irradiates the sample surface, the beam energy is dissipated through inelastic scattering within the interaction volume. During this energy dissipation, thermal waves are produced as a result of the heat generated. These thermal waves attenuate rapidly and this in turn leads to the generation of elastic acoustic waves [3], which propagate through the sample to the PZT detector for SEAM imaging. On the other hand, EBIC does not require modulation of the electron beam. The incident

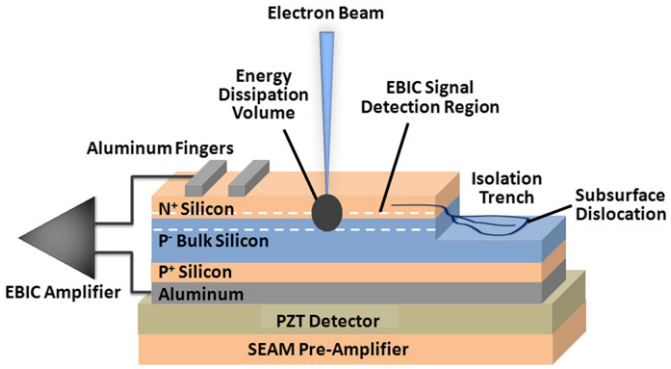

Fig. 3. EBIC signal detection of the solar cell.

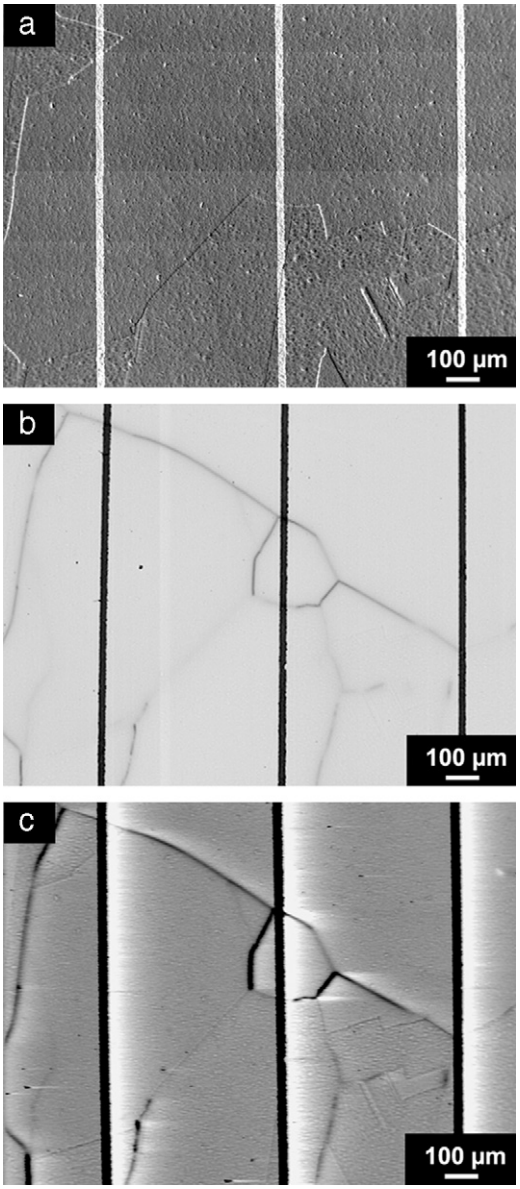

Fig. 4. (a) SE image at 30 KeV. The parallel lines are the aluminum contacts (b) EBIC image at 20 KeV; (c) SEAM amplitude image at 30 KeV and modulation frequency of 261 KHz. The SEAM image shows more defect features as compared to EBIC.

electron beam creates electron-hole pairs within the sample. When the electrons and holes are generated near a pn junction, they are separated by the electric field of the pn junction leading

to an EBIC signal. Both Figs. 2 and 3 also illustrate a defect, which appears as a subsurface dislocation that extends from the photovoltaic region into the isolation trench. As a result of the detection limit of EBIC mentioned previously, only the portion of the defect that is within several diffusion lengths of the pn junction can be observed by EBIC; the other parts of defect that extend further into the trench where pn junction is absent are not detectable by EBIC and only appear in the SEAM image.

3. Results and discussion

Fig. 4a is the secondary electron (SE) image of the solar cell device depicted in Figs. 2 and 3, while the corresponding EBIC and SEAM amplitude images are shown in Fig. 4b and c, respectively. Both the EBIC and SEAM amplitude images show strong contrast of similar defect features that are not observed in the SE image. This suggests that these defects are not near the sample surface; they are located at subsurface, at a distance that is larger than the mean-free-paths of the low-energy secondary-electrons, and are thus not detected in the SE image. Careful comparison of the EBIC and SEAM amplitude images reveals that some morphological defects shown in the SEAM image were not detected by EBIC. This difference can again be explained if such defects are not located within the EBIC signal detection range, as elucidated using the example of subsurface dislocations in Figs. 2 and 3. Another possible reason for the discrepancy is that not all the morphological defects are electrically active as this will be discussed later in detail. The difference between SEAM and EBIC can be better demonstrated using an isolation trench region (bottom right of Fig. 5a) of the solar cell. It can be observed from the EBIC image in Fig. 5b that no defects were detected in isolation trench while electrical defects are clearly evident in the solar cell region. This is expected as the pn junction is truncated at the trench for isolation purposes. On the other hand, in addition to picking up similar defect features in the cell region, both SEAM amplitude and phase images in Fig. 5c and d, respectively, also reveal the morphological defects in the isolation trench.

To better understand the origin of the subsurface defects in the isolation trench area, SEAM imaging is performed on the p^- silicon substrate wafer prior to the deposition of the n^+ silicon epitaxial layer and the aluminum contacts. EBIC analysis is not carried out on this sample as there is no EBIC signal without a pn junction. Prior to the SE and SEAM imaging, the silicon wafer was bathed in the alkaline solution of saw damage etch (SDE) for 20 s for saw damage removal and surface texturing. Fig. 6a and b show the SE and the corresponding SEAM amplitude images of the p^- Si wafer, respectively. The SEAM image shows defects in the p^- silicon substrate, implying that such morphological defects are originally present in the p^- silicon substrate and are not the result of the deposition of the n^+ film or the isolation trench formation. The morphological defects observed in the silicon substrate may impair the electrical performance of the photovoltaic device if they are located within few diffusion lengths of the pn junction after the formation of solar cells is completed.

Since morphological and electrical defects as revealed by SEAM and EBIC, respectively, are generally present in the poly-Si solar cells used in this work, the correlation between a morphological defect and its electrical activity is investigated. This is achieved by carefully performing SEAM and EBIC analysis on a photovoltaic region. Fig. 7a, b, c and d show the SE image, EBIC image, SEAM amplitude and phase images of the same region in a poly-Si solar cell. Firstly, a striking difference between the SEAM amplitude and phase images in Fig. 7c and d is observed. By comparing with the SE image in Fig. 7a, it can be easily seen that the SEAM amplitude image resembles the SE micrograph closely. In other words, SEAM amplitude mode reveals morphological defects that are located closer to the surface. This is expected as phase imaging is more sensitive to the material property in depth [8] and SEAM phase mode is therefore able to provide more subsurface details. Secondly, for most of the electrical defects observed in EBIC, morphological anomalies are detected by SEAM at the same location.

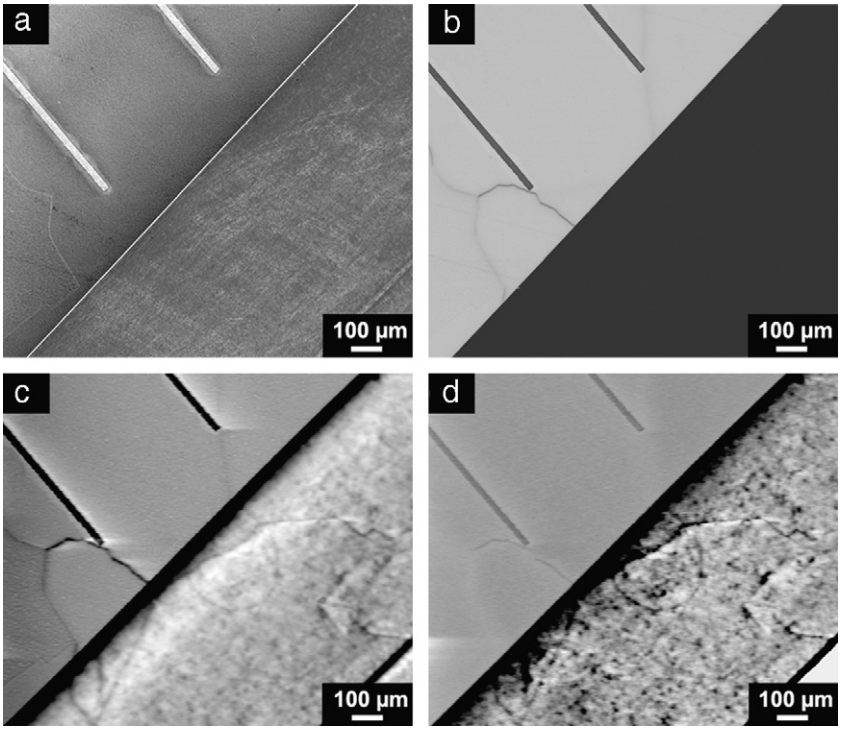

Fig. 5. (a) SE image and (b) EBIC image at 20 KeV; (c) SEAM amplitude image and (d) SEAM phase image at 30 KeV and modulation frequency of 363 KHz. No defect was detected in the isolation trench by EBIC.

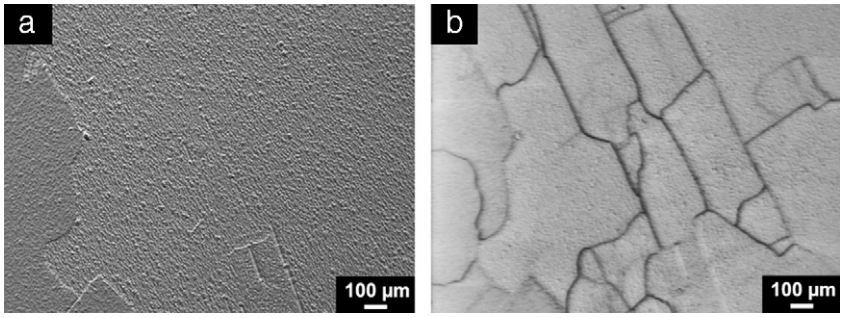

Fig. 6. (a) SE image and (b) SEAM amplitude image of p^- Si wafer before junction formation at 30 KeV and modulation frequency of 292 KHz.

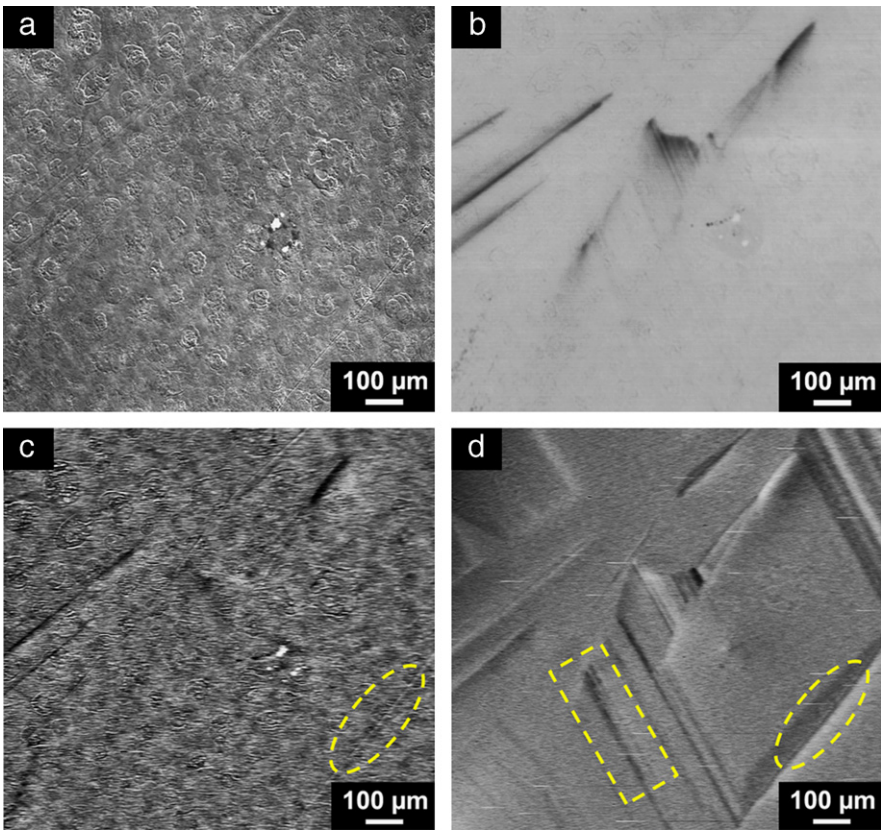

Fig. 7. (a) SE image at 30 KeV; (b) EBIC image at 20 KeV; (c) SEAM amplitude image and (d) SEAM phase image at 30 KeV and modulation frequency of 550 KHz. (For interpretation of the references to color in this figure legend, the reader is referred to the web version of this article.)

This means that most of the electrical defects detected are also morphological in nature. The opposite scenario is, however, not necessarily true as some morphological defects detected by SEAM are electrically inactive and cannot be observed by EBIC. For instance, a line-like defect (mostly probably a grain boundary) is clearly shown in both SEAM amplitude and phase images (circled in yellow) but is undetectable by EBIC. Furthermore, electrical properties can vary at different locations within a single morphological defect. A clear example in this case is the line-like defect in Fig. 7d (marked by the rectangular box) as EBIC signals decrease at only the top end but not the rest of the defect. Such variations of electrical activity within a single morphological defect observed in our experiment are not uncommon [9].

Fig. 8a and b show the EBIC and SEAM images, respectively, at another location of the same solar cell depicted in Fig. 5, whereas Fig. 8c is the line profiles of the signal contrast across the defects at $X-X'$ and $Y-Y'$ marked on the EBIC and SEAM images. The contrast of a signal is defined as the ratio of the signal intensity of the subsurface defects to the standard deviation of the surface background signals. After normalizing the intensity of surface background signals to zero for both line profiles, the subsurface defects show negative contrast. At $X-X'$, the signal contrasts of the defect from EBIC and SEAM line profiles are found to be -11.0 and -7.0, respectively, indicating that the defect is both morphological and electrical in nature. It is to be noted that the magnitudes of the EBIC and SEAM signal contrast in this case cannot be compared directly due to the different imaging parameters used. Interestingly, at $Y-Y'$, the signal contrast of the defect from the EBIC line profile is calculated to be -9.5 while the defect contrast from the SEAM signal line profile is barely observable. In other words, this defect is predominantly electrical in nature but without morphological features.

An experiment was performed to validate that a defect can be electrically apparent and yet morphologically invisible. A reverse-biased overstress was applied to a solar cell to intentionally create defects at the pn junction [10]. As a result of applying a 1 KV pulse,

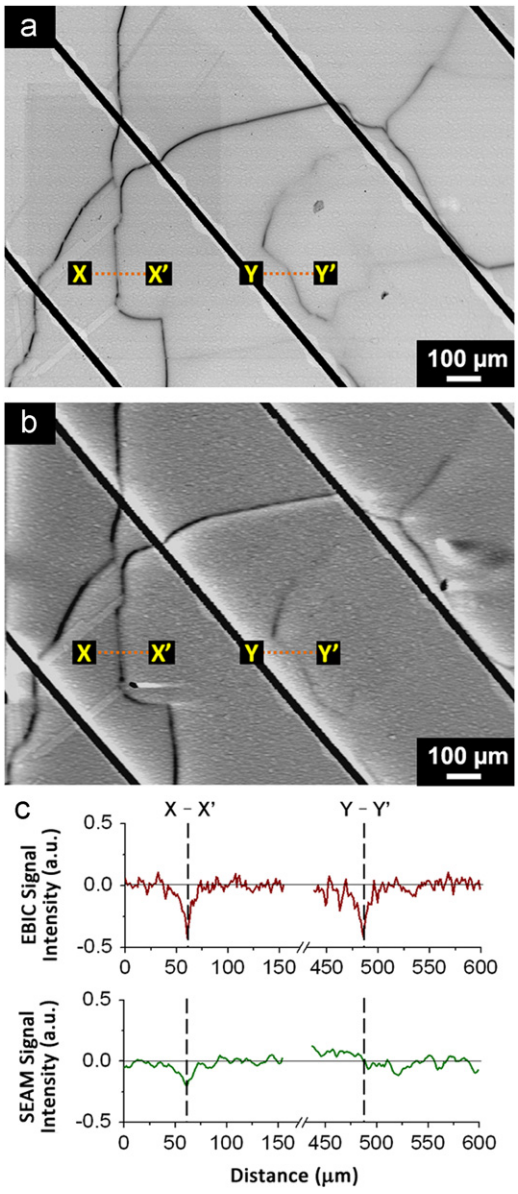

Fig. 8. (a) EBIC image at 20 KeV; (b) SEAM amplitude image at 30 KeV and modulation frequency of 391 KHz; (c) Line profiles at X – X′ and Y – Y′ of both EBIC and SEAM images.

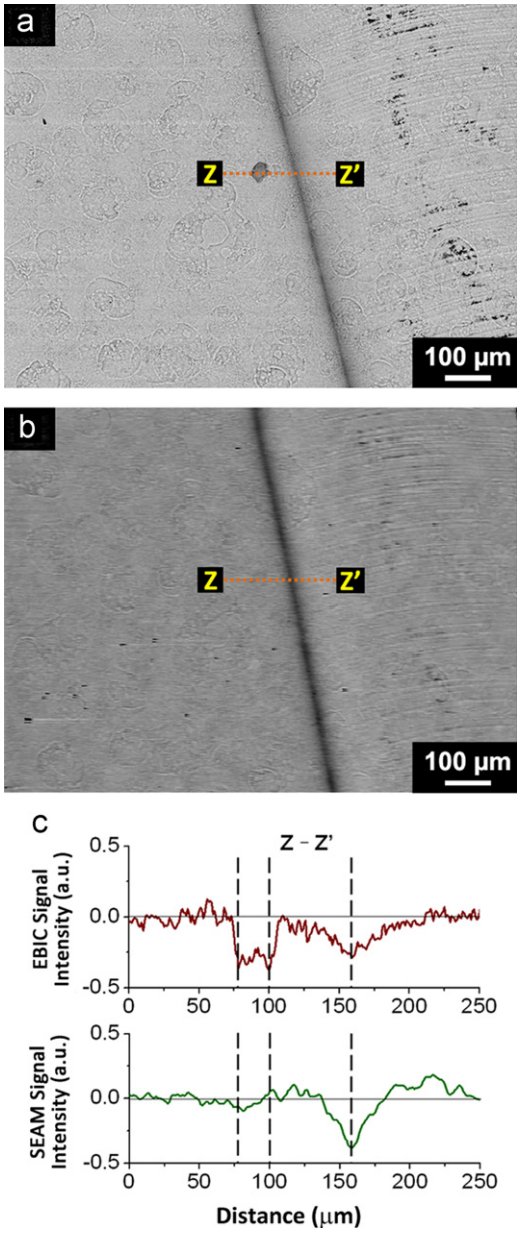

Fig. 9. (a) EBIC image at 20 KeV; (b) SEAM amplitude image at 30 KeV and modulation frequency of 292 KHz; (c) Line profiles at Z – Z′ of both EBIC and SEAM images.

the current–voltage (*I–V*) characteristics of the solar cell changed from a diode to a resistive short. Fig. 9a shows the EBIC image of the stressed solar cell revealing both a spot-like defect that is created by the electrical overstress and a line-like defect that is originally present in the solar cell before the overstress. On the other hand, Fig. 9b shows the SEAM amplitude image of the same location where only the line-like defect is clearly observable and matches that imaged by EBIC, indicating that the defect is morphological in nature. Fig. 9c illustrates the normalized signal intensity line profiles across the defects at Z – Z′ for both the EBIC and SEAM images. The EBIC line profile shows the spot-like defect with a width of 25 μm and a contrast of approximately −6.2 while the corresponding SEAM line profile does not show any appreciable contrast , which confirms that the spot-like defect is electrically active while not morphologically apparent. This defect is an electrical defect without morphology that is not detectable by SEAM.

In order to verify that the SEAM and EBIC techniques can indeed distinguish morphological and electrical defects, the cross-section of the defects along Z – Z′ shown in Fig. 9a and b was achieved after

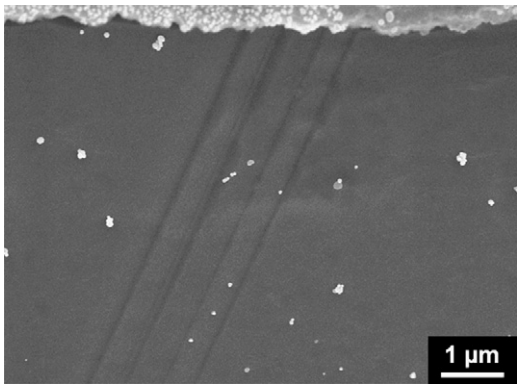

Fig. 10. SE image of the cross-section at the location of the line-like defect shown in Fig. 9a and b.

a 100 nm thick platinum layer was deposited on the sample surface using focused ion beam (FIB). Fig. 10 shows a SE image of the cross-section where dark oblique lines are observed to be located exactly at the morphological line-like defect that was originally present before the overstress. However, no apparent contrast can be seen at the location of the spot-like defect. It is clear that the spot-like defect, which is detected only by EBIC is an electrical defect whereas the line-like defect captured by both SEAM and EBIC is both morphological and electrical in nature.

4. Conclusions

The SEAM and EBIC techniques are successfully applied to distinguish morphological and electrical defects in polycrystalline silicon solar cells. It has been shown that while some defects are both morphologically and electrically detectable, some are apparent only either electrically or morphologically. Combining SEAM and EBIC is therefore an ideal approach as these two techniques are able to provide complementary information about defects, which may shed some light into the possible effects of the defects on the solar cell performance. Furthermore, SEAM and EBIC as complementary defect characterization techniques need not be limited to just poly-Si solar cells and can also be further extended to other materials and devices. With this method it is possible to further investigate the properties of the defects and their effects on solar cell quality and performance.

Acknowledgments

Samples for this project were provided by IBM Thomas J. Watson Research Center, Yorktown Heights, NY, USA, under the NUS & IBM Joint Study Agreement # W0853529. Funding and support from Qualcomm CDMA Technologies, San Diego, USA, under the NUS & Qualcomm Research Agreement # NAT-12150 is acknowledged. Funding for this research under Singapore National Research Foundation Grant # NRF2008EWT-CERP002-032 is acknowledged.

References

[1] Y. Yan, K.M. Jones, C.S. Jiang, X.Z. Wu, R. Noufi, M.M. Al-Jassim, Understanding the defects in polycrystalline photovoltaic materials, Physica B: Physics of Condensed Matter 401–402 (2007) 25–32.
[2] L.J. Balk, Scanning electron acoustic microscopy, Advances in Electronics and Electron Physics 71 (1988) 1–73.
[3] L.J. Balk, N. Kultscher, Nonlinear scanning electron acoustic microscopy, Journal de Physique Colloque C2 (2) (1984) 869–872.
[4] Y. Ohshita, Y. Nishikawa, M. Tachibana, V.K. Tuong, T. Sasaki, N. Kojima, S. Tanaka, M. Yamaguchi, Effects of defects and impurities on minority carrier lifetime in cast-grown polycrystalline silicon, Journal of Crystal Growth 275 (2005) e491–e494.
[5] H.J. Leamy, Charge collection scanning electron microscopy, Journal of Applied Physics 53 (1982) R51–R80.
[6] O. Breitenstein, J. Bauer, M. Kittler, T. Arguirov, W. Seifert, EBIC and luminescence studies of defects in solar cells, Scanning 30 (2008) 331–338.
[7] L. Meng, A.G. Street, J.C.H. Phang, Subsurface imaging of multi-level integrated circuits using scanning electron acoustic microscopy, in: Proceedings of international symposium testing and failure analysis (ISTFA), 15–19 November 2009, San Jose, California, USA, pp. 27–32.
[8] A. Rosencwaig, G. Busse, High-resolution photoacoustic thermal-wave microscopy, Applied Physics Letters 36 (1980) 725–727.
[9] J.I. Hanoka, Electron-beam-induced current characterization of polycrystalline silicon solar cells, Solar Cells 1 (1980) 123–139.
[10] R.L. Pease, J.R. Barnum, Silicon solar cell damage from electrical overstress, IEEE Transactions on Nuclear Science 29 (6) (1982) 1526–1532.